






Original Article


## Discharge evolution law of debris flow based on a sharp bend physical modeling test


LU Ming<sup>1,2,3</sup>  <https://orcid.org/0009-0000-5303-7737>; e-mail: luming20@mails.ucas.ac.cn

SUN Hao<sup>1,2\*</sup>  <https://orcid.org/0000-0001-9300-5553>;  e-mail: sunhao@imde.ac.cn

LIU Jinfeng<sup>1,2</sup>  <https://orcid.org/0000-0002-5542-827X>; e-mail: liujf@imde.ac.cn

Abrar HUSSAIN<sup>1,2,3</sup>  <https://orcid.org/0009-0006-6466-1192>; e-mail: abrar19960301@imde.ac.cn

SHANG Yuqi<sup>1,2,3</sup>  <https://orcid.org/0000-0003-3782-9499>; e-mail: 1121175654@qq.com

FU Hang<sup>1,2,3</sup>  <https://orcid.org/0009-0002-5621-8765>; e-mail: 1054279354@qq.com

\*Corresponding author

<sup>1</sup> Key Laboratory of Mountain Hazards and Earth Surface Process, Chinese Academy of Sciences, Chengdu 610041, China.

<sup>2</sup> Institute of Mountain Hazards and Environment, Chinese Academy of Sciences, Chengdu 610041, China.

<sup>3</sup> University of Chinese Academy of Sciences, Beijing 100049, China

**Citation:** Lu M, Sun H, Liu JF, et al. (2024) Discharge evolution law of debris flow based on a sharp bend physical modeling test. Journal of Mountain Science 21(6). <https://doi.org/10.1007/s11629-023-8434-6>

© Science Press, Institute of Mountain Hazards and Environment, CAS and Springer-Verlag GmbH Germany, part of Springer Nature 2024

**Abstract:** For the basins with debris flow development, its channel terrain exhibits a tortuous shape, which significantly restricts the movement of debris flows and leads to severe erosion effects on the concave bank. Therefore, this study aims to analyze the shear force of debris flows within the bend channel. We established the relationship between the shear force and bend curvature through laboratory experiments. Under the long-term erosion by debris flows, the curvature radius of bends gradually increases, however, when this increasing trend reaches an equilibrium state with the intensity of debris flow discharge, there will be no significant change in curvature radius. In general, the activity pattern and discharges of debris flows would remain relatively stable. Hence, we can infer the magnitude of debris flow discharges from the terrain parameters of the bend channel.

**Keyword:** Debris flow discharge; Erosion effect; Bend channel; Curvature radius

### 1 Introduction

Debris flows are a common geological hazard in mountainous regions, it can transport large amounts of sediment to the accumulation areas in a relatively short time (Zheng et al. 2021a). In recent years, the number of debris flow disasters increase significantly with a growing number of populations in mountainous regions, as well as rapid climate changes, earthquakes and other factors (Stoffel et al. 2014; Zheng et al. 2021b). Debris flow's erosion process could expose the foundation of the building, widening the cross-sectional shape of the channel, etc. There were numerous field observations suggesting that debris flows have a greater erosion capacity than water or sediment-laden water (Zheng et al. 2018; Zheng et al.

**Received:** 25-Oct-2023  
**1<sup>st</sup> Revision:** 25-Dec-2023  
**2<sup>nd</sup> Revision:** 14-Mar-2024  
**Accepted:** 26-Mar-2024

2021b; Pan et al. 2015), the activity pattern of large fluctuations in discharges was also found to be associated with the debris flows. During the flow from the initiation zones to the accumulation zones, debris flows continuously erode the channel, while also significantly modifying the channel topography (Rickenmann et al. 2003; D'Ambrosio et al. 2007), therefore, the evolution of channel geomorphology can reflect the debris flow activities pattern.

Widespread scholars believe that the final volume and maximum discharge of debris flows are important parameters to assess the disaster scale and the maximum accumulation range (Dowling and Santi, 2014; Roelofs et al. 2022). At present, there are rain flood method and in-site investigation of post disaster to determine the discharge of debris flow, and then evaluate the final total volume of debris flow in combination with the disaster duration (Hu et al. 2010; Kim et al. 2018). However, the rain flood method belongs to the semi empirical method, which may affect the calculation accuracy due to human subjectivity. Secondly, due to the accidental characteristic and most disasters location at inaccessible mountainous areas, in-situ investigation is almost impossible (Chen et al. 2007).

Due to the slight erosion process on the channel bank by debris flow, most research focuses on the erosion phenomenon of channel bed (Frank et al. 2015; Han et al. 2015; Iverson et al. 2012; Kean et al., 2015; Haas et al. 2022), but this conclusion only applies in the case of straight channels. Under the bend channel situation, centrifugal acceleration occurring, and strongly erodes the concave bank. Although bank erosion is not as severed as bed, bank erosion (destruction of the slopes foot) is the main reason of slope instability (Gonzalez-Diez et al. 1999; Lacoste et al. 2011; Larsen and Montgomery 2012; Doi et al. 2020), the collapse and damage of the slope not only provide loose soil for debris flows, but cause the shoreline moving back and accelerate the terrain evolution.

The debris flow's discharge is determined based on local geological, geographical, geomorphological, and climatic conditions, etc.. In regard to the downstream part of channels, the discharge of debris flow is often closely related to the curvature radius of the bend. Because the erosion ability of debris flow on the concave bank is mainly controlled by the curvature radius of the bend, when the curvature radius of the bend is increased sufficiently under debris flow erosion

processes, the erosion ability of debris flow would be weakened. When this relationship reaches a certain equilibrium state, the curvature radius of the bend wouldn't increase significantly.

This paper studies the relationship between the erosion ability of debris flow on the concave bank and the curvature radius of the bend. On this basis, we take the Fencha Gully as an example, and conduct a detailed analysis of the relationship between debris flow's discharge and the terrain of bend channels, finally, the discharge of debris flow in the Fencha Gully was calculated. In conclusion, this paper can provide a new approach for estimating the discharge of debris flows.

## 2 Material and Method

### 2.1 Scale analysis

The erosion that occurred on the concave bank was induced by centrifugal acceleration motion, which was mainly determined by the debris flow's velocity and the curvature radius of bend channels. The curvature radius scale is given by the ratio of the curvature radius  $R_c^*$  of the field prototype to the curvature radius  $R_c$  of the model bend in the laboratory.

$$L = \frac{R_c^*}{R_c} \quad (1)$$

The channel width scale  $W$  is given by the ratio of prototype trench width  $B^*$  to the model channel width  $B$ :

$$W = \frac{B^*}{B} \quad (2)$$

The terrain parameters of bend curvature radius  $R_c$  and channel width  $B$  are important factors for the centrifugal acceleration. Therefore, we proposed a dimensionless bend parameter  $\lambda$ , which was given as the ratio of curvature radius  $R_c$  to channel width  $B$ :

$$\lambda = \frac{B}{R_c} \quad (3)$$

The bend parameter  $\lambda$  in model experiment are consistent with the prototype  $\lambda^*$ :

$$\lambda^* = \lambda \quad (4)$$

The Froude number ( $F_r$ ) is an important dimensionless parameter, it indicates the kinetic energy component ratio between horizontal and vertical directions. We applied dynamic similarity to our experiment using the  $F_r$  scaling concept.

$$F_r = \frac{v^*}{\sqrt{gh^*}} = \frac{v}{\sqrt{gh}} \quad (5)$$

where,  $v^*$  and  $v$  is debris flow velocities in the prototype and experiment, respectively;  $g$  is the gravity acceleration;  $h^*$  and  $h$  is the depth of the mud level in the prototype and experiment, respectively. The value

**Table 1** Parameters value in the laboratory and the prototype situation

Situation	$R_c$ (m)	$B$ (m)	$\lambda$	$v$ (m/s)	$h$ (m)	$F_r$
Laboratory	1.30-2.00	0.3	0.15-0.23	2.1-4.1	0.060-0.090	2.3-4.9
Prototype	52.00	14.0	0.17	5.5-8.5	0.150-0.350	3.5-5.0

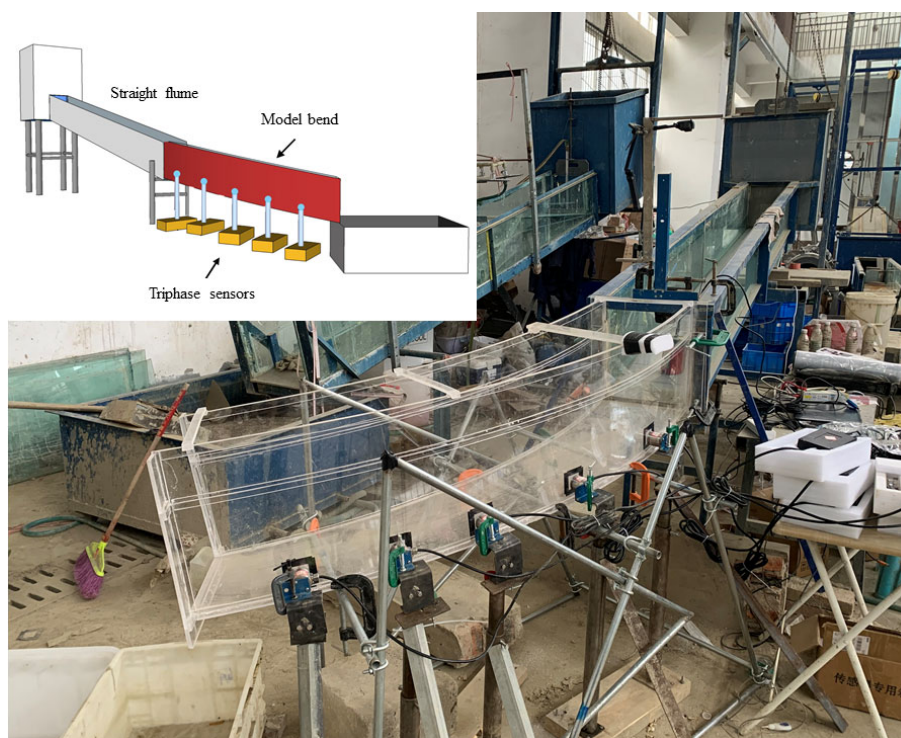


**Fig. 1** Schematic diagram of model testing device.

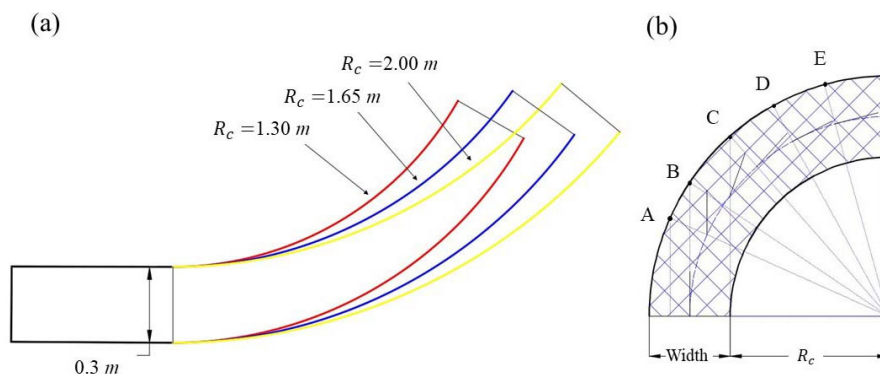


**Fig. 2** Schematic diagram of the model curve (a) bend models of different sizes; (b) sensor mounting position.

ranges for these parameters are listed in [Table 1](#).

## 2.2 Experimental equipment and devices

As shown in [Fig. 1](#), the structure of the flume experiment consists of a hopper, straight flume, model bend, and tailings box. The data acquisition equipment

consists of sensors, sensor brackets, data acquisition system, and mud level meters. The hopper size is 600 mm × 600 mm × 900 mm, with a straight flume size of 4000 mm × 300 mm × 400 mm was used to through the stirred debris flow to the model bend. The width of the model bend is 0.3m, and its curvature radius was 1.30 m, 1.65 m, and 2.00 m ( $R_c$  is the length from the center to the convex bank of the bend), respectively. The size of the tailings pond is 900 mm × 900 mm × 450 mm, which was used to collect debris flow samples. Triphasic sensors could measure the magnitude and direction of the impact force of debris flow, which were installed at the bottom of the concave bank. The sample frequency of the data acquisition instrument is 1000 Hz. The sampling frequency of laser mud level meter is 1000 Hz, measurement accuracy is 0.1 mm. A high-speed camera (GoPro) was used to record the entire experimental process, with a shooting frequency of 240 frames/s.

As shown in [Fig. 2](#), there were three different size bend models, their width is 0.3 m and height is 0.4 m. In the field, the foot of the concave bank was eroded



and damaged frequently by debris flows, so sensors were installed at the bottom of the concave bank.

### 2.3 Experiment material

The debris flow materials were collected from the debris flow accumulation area in the Fenchu Gully, located in Xide County, Sichuan Province. During the sampling process, the particles with a particle size exceeding 40 mm were filtered out. The characteristics of particle size of the material is  $d_{95} = 29.44$  mm, the median particle size is  $d_{50} = 2.7$  mm,  $d_{30} = 0.12$  mm. The grading curve of particle is shown in Fig. 3.

### 2.4 Sensor arrangement

Five sensors were installed on bottom of concave bank, different installed location represents different erosion mechanisms by debris. Point A and Point B represent the initial stage of debris flow within the bend and it hasn't transformed into centrifugal motion completely. Points D~E represent that the debris flow has transformed to centrifugal motion completely, and during this stage. The sensor probes are completely flush with the concave bank sidewall and it located at the center of the hole (Fig. 4). A plastic film is attached to the surface of the hole to prevent small particles embedding into the gap between the probe and the hole. As shown in Fig. 4(b), the sensor is installed on a specially bracket, which can move up and down and rotates horizontally to ensure that the sensor probe is accurately installed in the center of the hole. The control variables of the model experiment are debris flow density, straight flume slope, and curvature radius of model bend. There are 6 different debris flow densities ( $\rho=16, 17, 18, 19, 20, 21$  kN/m<sup>3</sup>), 4 straight flume slopes ( $\theta=9^\circ, 11^\circ, 13^\circ, 15^\circ$ ), and 3 model bends ( $R_c=2.00, 1.65, 1.30$  m), and every variable intersecting with each other to conduct experiments.

## 3 Theoretical Model

### 3.1 Centrifugal force of debris flow on concave banks

Through model experiments, the centrifugal force of debris flow can be measured. Therefore, by dimensionless the peak centrifugal force of debris flow, we can get the relationship between fitting coefficient

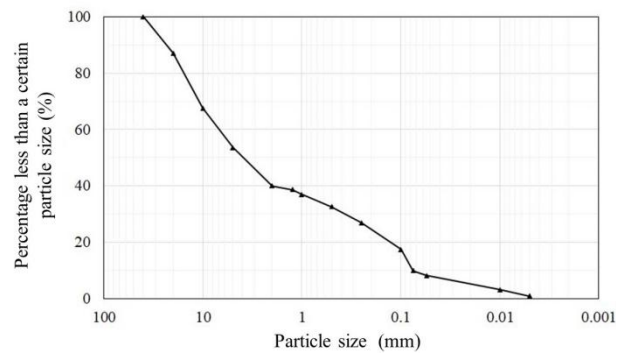


Fig. 3 Preparation of debris flow material sampling.



Fig. 4 Schematic diagram of sensor installation: (a) sensors installed at the bottom of the concave bank (b) sensor bracket.

$\alpha$  with bend parameters  $\lambda$  and  $F_r$ :

$$\alpha = \frac{\sigma_{max}}{\rho v^2} = f(\lambda, F_r) \quad (6)$$

where,  $f(\lambda, F_r)$  is a function with the bend parameters and Froude number, and the form of the function is determined through experimental data.

### 3.2 Relationship between debris flow's discharge and shear force

As shown in Fig. 5, during the motion process within the bend channels, The movement direction of debris flow changes gradually, from straight motion transition to centrifugal motion. And it would cause destabilization and failure of bank soils. The cross-section of the debris flow body also changes from square to triangle. In some studies, it was believed that the cross-sectional shape when passing through bends was trapezoidal, but according to the practical phenomenon in this experiment, the cross-section of the debris flow should present a triangle shape. We

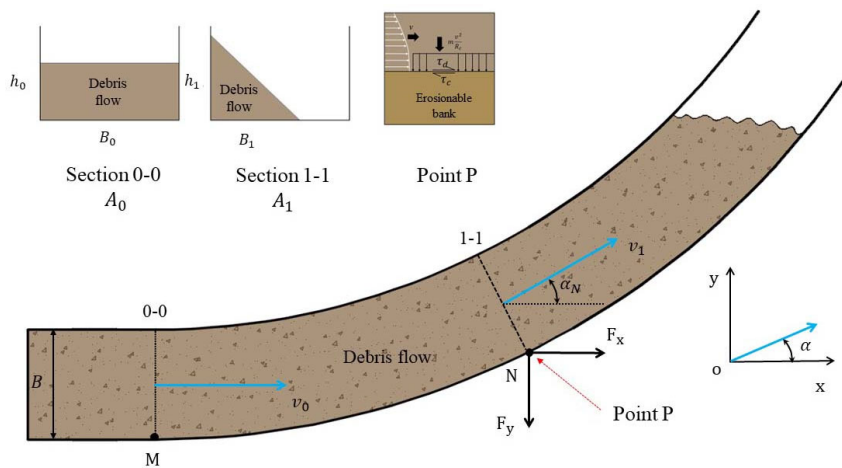


**Fig. 5** Schematic illustration of debris flow’s erosion process within bend channel.

assumed that the debris flow’s velocity at section a-a is  $v_0$ , and the flow velocity at section b-b is  $v_1$  (the subscript with “0” indicates the state which the debris flow hadn’t entered the bend, and the subscript with “1” indicates the state that the debris flow had entered the bend).

As shown in Fig. 5, section 0-0 and section 1-1 are the cross sections of debris flow before and after entering the bend respectively. We take the process of debris flow from point M to point N as the research object, because the direction of debris flow gradually deviates to the concave bank, so it is assumed that the convex bank does not have a limiting effect on debris flow movement. The coordinate system is established based on the x and y axis directions as shown in Fig. 5. Therefore, the continuity equation and mass equation of the debris flow movement process between M and N are as follows:

$$F_y = v_1 \sin \alpha q_{m1} - 0 \cdot q_{m0} \quad (7)$$

$$F_x = v_1 \cos \alpha q_{m1} - v_0 q_{m0} \quad (8)$$

$$q_{m0} = q_{m1} \quad (9)$$

where,  $q_{m0} = \rho A_0 v_0$ ,  $q_{m1} = \rho A_1 v_1$ ,  $\rho$  is density of debris flow;  $A_0, A_1$  is the fluid cross section area at point M and point N, respectively;  $F_y$  is the force on the concave bank in the M~N segment along the y axis;  $F_x$  is the force on the concave bank in the M~N segment along the x axis;  $\alpha$  is the Angle between the debris flow velocity and the direction of x axis at a point N.

Since the distance between points M to N is relatively short compared with the length of the whole debris flow movement process, the influence of gravity work and friction force on debris flow velocity in the analysis of debris flow movement in this stage is not considered. Therefore, according to the Bernoulli's

formula, the flow velocity of debris flow at points M and N is equal, namely:

$$v_0 = v_1 \quad (10)$$

This is obtained by formula 10:

$$\rho A_0 v_0 = \rho A_1 v_1 \quad (11)$$

Therefore, after combining the Bernoulli formula and mass conservation formula analysis, although the cross-section shape of debris flow fluid at points M and N changes, its cross-section area remains unchanged:

$$B_0 h_0 = 0.5 B_1 h_1 \quad (12)$$

Combined with formula 8 and 9, the resultant debris flow force on the concave bank in section M~N is as follows:

$$F_{sum} = \sqrt{F_x^2 + F_y^2} = \rho v^2 B_0 h_0 \sqrt{2 - 2 \cos \alpha} \quad (13)$$

where,  $F_{sum}$  is the resultant force of debris flow on the concave bank in the M~N segment;  $v$  is the flow velocity of the debris flow;  $B$  is the width of the straight channel;  $h_0$  is the depth of mud when the debris flow comes.  $B_0$  is the section width of incoming debris flow, and its value is equal to the width of ditch  $B$ .

Combined with the analysis of the movement of the whole debris flow in the bend channel and the process of exerting force on the concave bank, the force of debris flow on each point of the concave bank is different, and the force is mainly affected by the Angle between the velocity direction and the x axis. Therefore, the resultant force of debris flow  $F_{sum}$  on the whole M~N segment of the concave bank can be calculated by the following formula:

$$F_{sum} = \int_0^{\alpha_N} g(\alpha) d\alpha \quad (14)$$

where,  $\alpha_N$  is the angle between the tangent line of the concave bank at point N and the x-axis, that is, the Angle between the direction of debris flow velocity and the x-axis;  $g(\alpha)$  is the function relationship between the debris flow force of a single point on the concave bank and the tangent angle  $\alpha$  of the concave bank at that point.

Therefore, a single point on the concave bank subjected to debris flow can be calculated by the following formula:

$$g(\alpha) = F'_{sum} = \frac{\sqrt{2}}{2} \rho v^2 B_0 h_0 \frac{\sin \alpha}{\sqrt{1 - \cos \alpha}} \quad (15)$$

where, the value of  $\alpha$  is mainly determined by the position of the calculation point, and the value range is  $0^\circ \sim 90^\circ$ .

We can get from Fig. 5, the fluid cross section of debris flow in the bend is triangular, so the debris flow force at point N (the longitudinal direction of the entire ditch bank) is as follows:

$$F_{N-sum} = \frac{1}{2} P_d h_1 \quad (16)$$

$$F_{N-sum} = g(\alpha_N) \cos \theta_N \quad (17)$$

where,  $F_{N-sum}$  is the force (N) affected by debris flow at Point N;  $P_d$  is the impact pressure (Pa) of debris flow to Point N.  $h_1$  is the height of the mud level of the debris flow at Point N, that is, the ultra-high height of the bend;  $\theta_N$  is the Angle between the debris flow force at Point N and the normal direction of the point. Because the flow process of debris flow in the bend is very complicated, and the direction of the force changes from time to time, the direction of the debris flow force at the concave bank in section M to N is replaced by the direction of the debris flow force at Point N in this study.

What we need to analyze is the relationship between the maximum curvature radius of the bend and the erosion capacity of the debris flow within the bend. Therefore, when the shear force of the debris flow is not enough to erode the concave bank of the bended channel, the curvature radius of the bended channel will not increase, that is:

$$\tau_{res} = n_c P \quad (18)$$

where,  $n_c$  is the roughness ratio of the ditch bank of the bend, which is determined by the nature of debris flow and the specific situation of the ditch bank, and the value here is 0.65;  $\tau_{res}$  is the shear strength of soil on the ditch bank.

By combining the correlation equations, a binary system of equations about ( $h_0, v$ ) two unknowns can be obtained:

$$\tau_{res} = P_1 \times n_c = 1.686 F_r^{-1.47} \lambda^{0.36} \rho v^2 \times n_c \quad (19)$$

$$\tau_{res} = P_d \times n_c = \sqrt{2} \xi \rho v^2 B \frac{h_0}{h_1} \frac{\sin \alpha}{\sqrt{1 - \cos \alpha}} \times n_c \quad (20)$$

where,  $\xi$  is the correction factor considering the uneven distribution of the pressure exerted by the debris flow on the ditch bank in the vertical direction, the value here is 0.65. After the  $h_0$  and  $v$  values in the basin are calculated, the flow of debris flow before it enters the

bended channel can be calculated by the following formula:

$$Q_0 = B h_0 v \quad (21)$$

where,  $Q_0$  is the average flow when the debris flow does not enter the bend.

## 4 Experimental Results

### 4.1 Interaction between the debris flow and concave bank

As shown in Fig. 6, the experiment process of debris flow impacts different bend banks under the same density ( $\rho=19 \text{ kN/m}^3$ ) and slope conditions ( $\theta=11^\circ$ ). Under the same velocity condition, smaller curvature radius of the bend would yield stronger limiting effect on the movement of the debris flow. At the same time, the debris flow will generate a higher super-elevation value, it would also exert greater force on the concave bank, which would result in significant increasing of force acting on the concave bank with increasing curvature radius.

As shown in Fig. 7, the experimental process of debris flow impacts the same curvature radius of bend ( $Rc=1.65 \text{ m}$ ) and slope conditions ( $\theta=11^\circ$ ) under different debris flow density conditions. The super-elevation value generated by  $21 \text{ kN/m}^3$  was less than  $\rho=16 \text{ kN/m}^3$  conditions. High density debris flow has a slower climbing speed and a smaller undulation angle in the cross section, while low density debris flow has a more intense impact process and a larger undulation angle in the cross section. However, small density debris flow with lower solid content inside the fluid, which results in a weaker erosion ability. When the density of debris flow is relatively high, a layer of viscous slurry would be covered on the surface of the bank, which would provide a lubrication and reduce the erosion intensity by debris flow.

### 4.2 Time-dependent evolution of debris flow impact force

The impact force of debris flow can be decomposed into x, y, and z directions. As shown in Fig. 8, the force was mainly reflected in the z axis, and the x axis also has noticeable fluctuation, but the force on the y axis present a weak state, which was mainly related to the debris flow motion characteristics. The force on the z-axis represents centrifugal force, and the



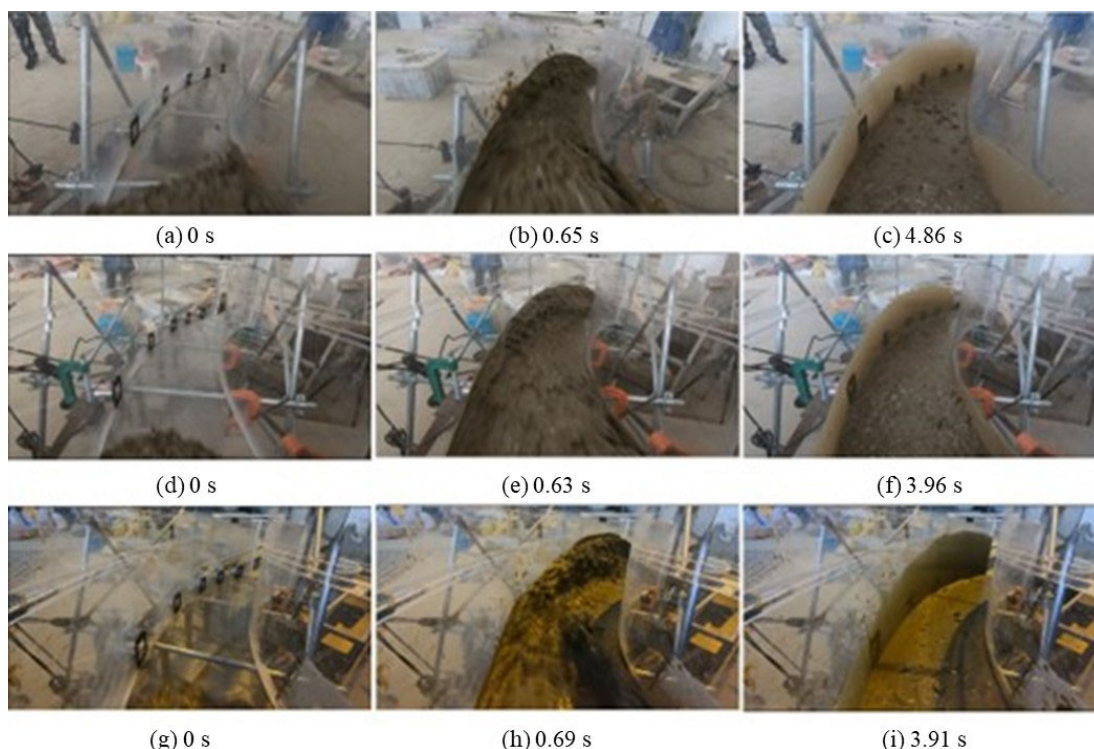


**Fig. 6** Process of debris flow impacting the concave bank at different bend curvature (a-c:  $R_c=2.00$  m, d-f:  $R_c=1.65$  m, g-i:  $R_c=1.30$  m).

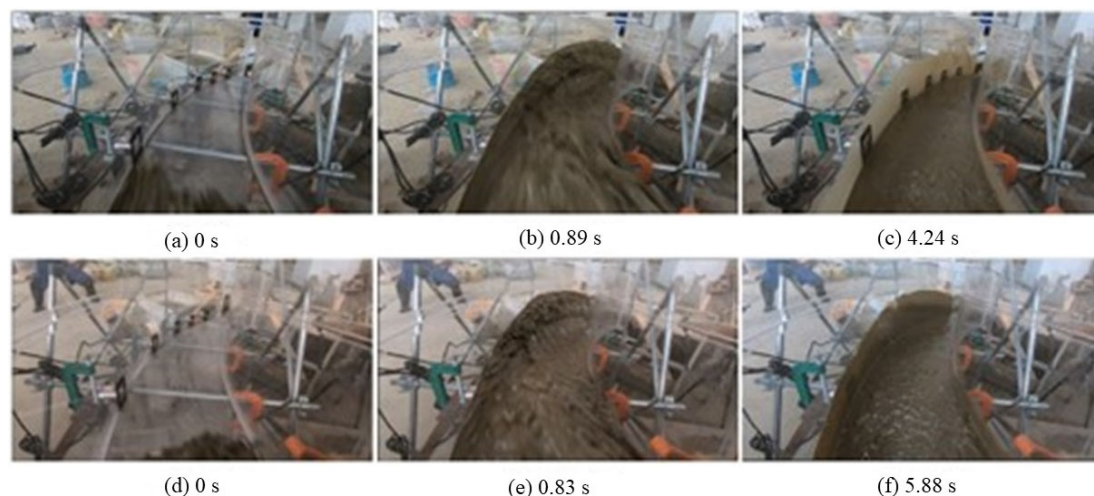


**Fig. 7** Process of debris flow impacting the concave bank under different density conditions (a-c:  $\rho=16$  kN/m<sup>3</sup>, d-f:  $\rho=21$  kN/m<sup>3</sup>).

force on the x-axis represents a shear force.

As shown in Fig. 9, the spatial distribution of peak centrifugal force at 5 different positions. In general, the centrifugal force at Point B was maximum, there was no significant difference in centrifugal force values between Point D ~ E. Point B was located at the intersection of the forward direction of debris flow with the concave bank, as shown in Fig. 2(a), due to the robust straightness of the debris flow movement, the

debris flow hasn't completely transformed into centrifugal motion at this stage, so the force at Point B was the impact force rather than the centrifugal force. When the debris flow reached the area of Points D ~ E, debris flow had ultimately transformed into centrifugal motion, and the magnitude of the force totally depends on the centrifugal acceleration, therefore, the force values at Points D ~ E area were nearly identical.

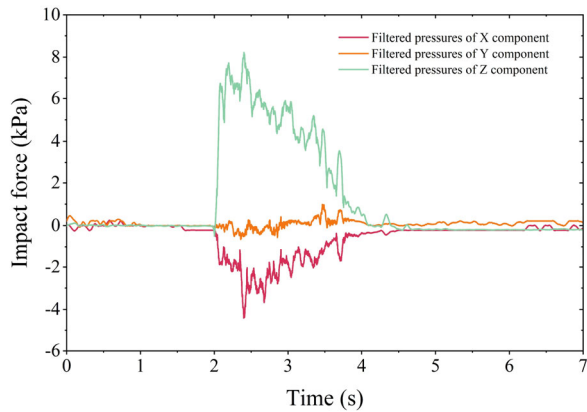


**Fig. 8** Components of the impact force on the x, y, and z directions,  $\lambda=0.23$ ,  $\rho=19 \text{ kN/m}^3$ ,  $\theta=15^\circ$ .

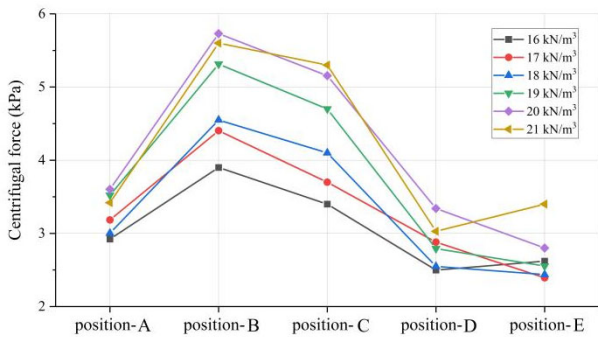


**Fig. 9** Peak centrifugal force distribution at different points on the concave bank;  $\lambda=0.23$ ,  $\theta=9^\circ$ .

### 4.3 Temporal distribution law of centrifugal force

Numerous field observations indicated that debris flow tends to exhibit linear movement. Consequently, when encountering buildings, debris flows can cause significant damage due to their powerful impact (Song et al. 2021; Ng et al. 2016). The concave bank will also undergo shear damage from the debris flow while gradually imposing constraints and altering the directions of the debris flow's motion. Therefore, the magnitude of the constraints imposed by bend on the debris flow also governs the shear force exerted by debris flow on the concave bank. This paper proposes  $\lambda$  as an index to measure the influence of curved terrain on the debris flow movement process. As shown in Fig. 10, it can be observed that  $\lambda=0.23$  exhibits a higher centrifugal force trend compared to  $\lambda=0.18$ ; however, the entire process of  $\lambda=0.23$  displays significant fluctuations and unstable pattern, the increased limiting effect of the bend has closely linked with this phenomenon.

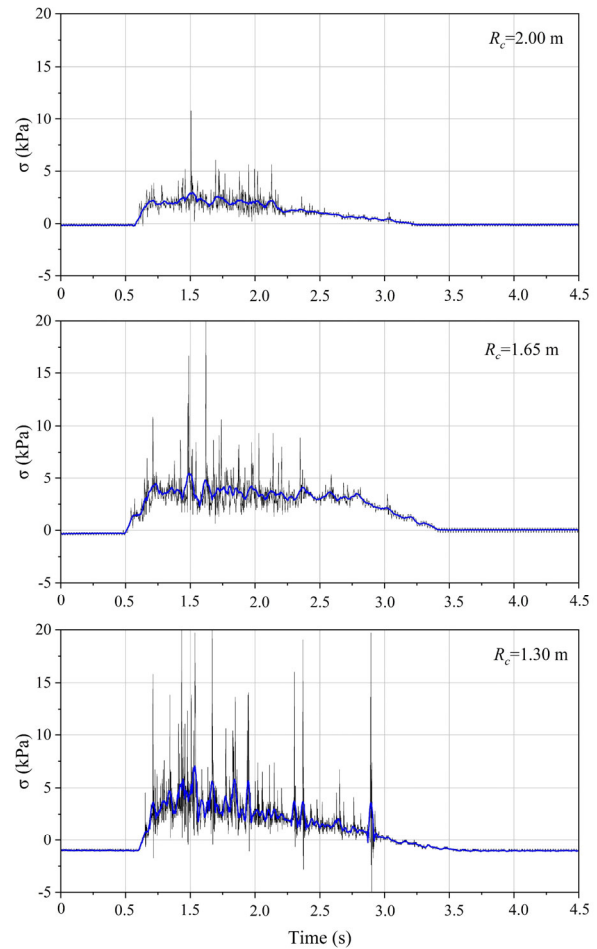


**Fig. 10** Shear force on concave bank under different curvature parameters of bend,  $\rho=16 \text{ kN/m}^3$ ,  $\theta=13^\circ$ .

### 4.4 Relationship between centrifugal force and the bend

The debris flow within the area of Points D~E transformed into centrifugal motion, and the predominant force acting on Points D~E was the centrifugal force (It was the component force on the Z-axis). A higher centrifugal acceleration leads to an increased positive centrifugal force on the concave bank, and the fast-moving fluid generates a shear force that erodes and damages the slope toe of the concave bank. Some experts have attempted to utilize the Froude number to correct dynamic pressure (Hübl et al. 2003; Tiberghien et al. 2007). In this paper, we made the centrifugal force dimensionless, as shown in Fig. 11. Finally, it can be concluded that there exists a relatively consistent power function relationship between dimensionless centrifugal forces and  $F_r$ .

We found that the dimensionless centrifugal force



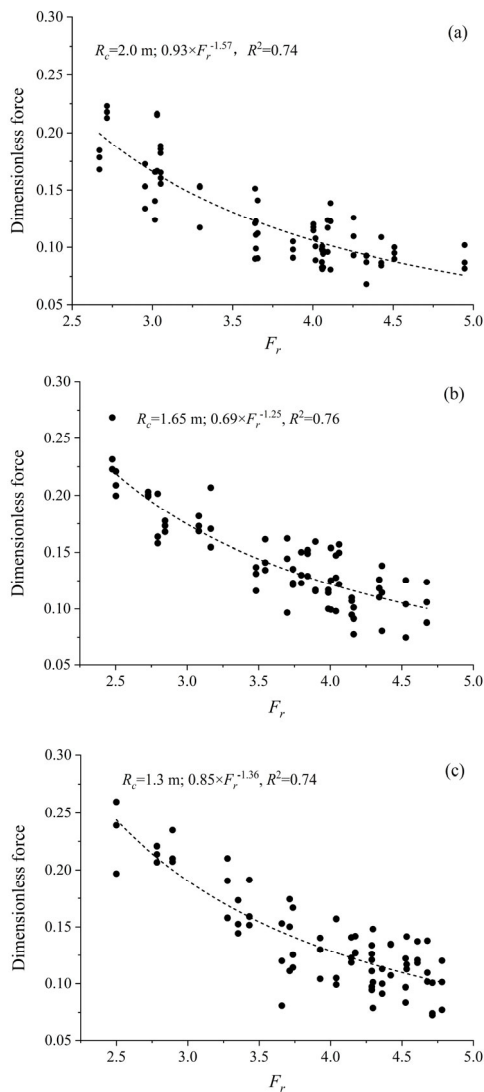


**Fig. 11** Relationship between dimensionless centrifugal force and  $F_r$ , (a)  $R_c=2.00$  m; (b)  $R_c=1.65$  m; (c)  $R_c=1.30$  m.

and  $F_r$  exhibit a power function relationship under different curvature radius conditions. From the previous analysis, it can be concluded that the decreasing of curvature radius, the more restricted of the bend for debris flow movement, finally debris flow would generate greater centrifugal force. Therefore, we analyzed all data under different curve conditions and finally obtained the bend parameters  $\lambda$  and the Froude number were power function relationship with  $\alpha$ , Eq. 12 is the specific function form is as follows.

The conclusion can be drawn that with the decreasing in curvature radius, it would induce more restrictive effect for debris flow movement, the shear force on the concave bank would exhibit a higher magnitude eventually. Consequently, the fitting

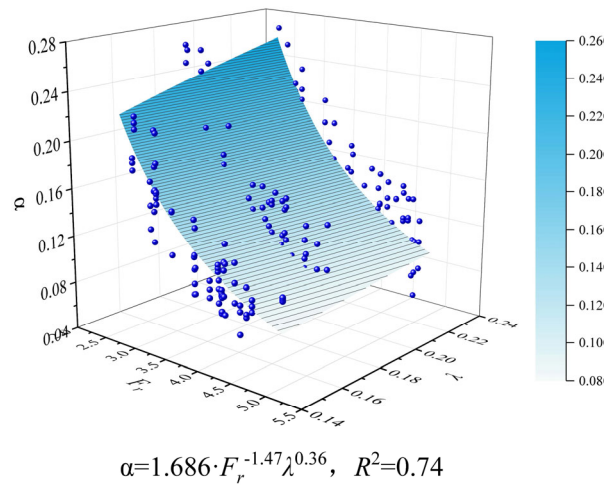


**Fig. 12** Fitting relationship of  $\alpha$  and  $\lambda, F_r$ .

analysis was conducted for the entire data under every curvature condition to establish the fitting relationship between the bending parameter  $\lambda, F_r$  and the dimensionless parameter  $\alpha$ . The fitting analysis results were shown in Fig. 12, and the fitting equation was shown as follows:

$$\alpha = 1.686 \times \lambda^{0.36} F_r^{-1.47} \quad (22)$$

## 5 Case Study

### 5.1 Background of Fencha Gully

Fencha Gully is located in the middle reaches of the Reshui River, which is located in Liangshan Prefecture, Sichuan Province. As show in Fig. 13, the watershed area of Fencha Gully is 0.38 km<sup>2</sup>, the length of the main channel is 846 m, which is distributed in the NW-SE direction. The highest position in the watershed is 2150 m, which is 284 m higher than the accumulation zone. The upstream topography of Fencha Gully exhibits a prominent steepness, where spread many landslides. The average annual rainfall is 1012 mm, the rainy season is from May to October every year, the total rainfall in the rainy season accounts for 88.4% of the total rainfall. The activity traces of debris flow in the Fencha Gully are obvious, furthermore an accumulation fan with volume of 5.4×10<sup>8</sup> m<sup>3</sup> had formed at the downstream.

### 5.2 Design discharge of debris flow

Due to the absence of available data about debris flow activity in the Fencha Gully, the debris flow's



**Fig. 13** Overview of the Fencha Gully.

discharge cannot be calculated according to the mathematical statistics method. According to the rainstorm and flood calculation manual for small and medium-sized basins. We calculated the design flood discharge, and then the debris flow discharge was calculated using the matching method. The calculation formula is as follows:

$$Q_d = D_u(1 + \varphi_d)Q_B \quad (23)$$

$$\varphi_d = \frac{(\rho_d - \rho_w)}{(\rho_s - \rho_d)} \quad (24)$$

where,  $Q_d$  is design discharge of debris flow,  $Q_B$  is the design clear water discharge,  $D_u$  is the blockage coefficient, with a value range of 1.5~3.0, which is determined based on the blockage situation of the channel in the basin;  $\varphi_d$  is the increase coefficient for debris flow.  $\rho_d$ ,  $\rho_w$ ,  $\rho_s$  are densities of debris flow, clean water, and solid matter, respectively.

We calculated the discharge of rainstorm under the different rainfall frequencies of 1%, 2%, 5% and 10%, and then the corresponding discharge of debris flow would be calculated, the calculation results have shown in [Table 2](#).

### 5.3 Estimation of debris flow's discharge according to the terrain parameters

In the mountainous regions, debris flow channels often exhibit a sinuous trend, and the significant erosion impact by debris flow on the concave bank would result in channels exhibit a more meandering shape. As discussed above, the shear force exerted by debris flow on the concave bank gradually diminishes as the curvature radius of the bend increases. Once a

state of an equilibrium is reached between shear force and resistance strength of bank, there wouldn't have substantial increase in the curvature radius of the bend, thus forming a topography could reflect the discharge characteristics of debris flow, however, the discharge of debris flow serves as an essential parameter for assessing debris flow activities.

**Table 2** Parameters of debris flow under different rainfall frequency in the Fencha Gully

Rainfall frequency (%)	$D_u$	$\varphi_d$	$Q_B$ (m <sup>3</sup> /s)	$Q_d$ (m <sup>3</sup> /s)
1	2.4	2.20	10.70	82.18
2	2.2	1.67	9.28	54.44
5	2.2	1.29	7.48	37.61
10	2.0	1.00	6.12	24.48

**Notes:** Rainfall frequency is the occurring probability of a specific rainfall intensity, which is closely related to the climatic conditions. The rainfall frequency is 1%, indicating that rainfall intensity is "once in a century". The lower the rainfall frequency, the greater the rainfall intensity.

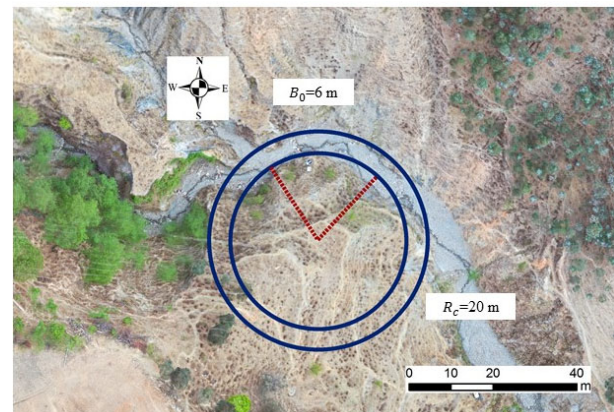


**Fig. 14** Bend channel at middle region of the watershed.

**Table 3** Calculation parameters of debris flow discharge

Variable (input)	$\rho$ (kN/m <sup>3</sup> )	$n_c$	$\tau_{res}$ (kpa)	$R_c$ (m)	$B$ (m)	$\lambda$	$\alpha_N$
Value	2050	0.65	27	20	6	0.3	40
Variable (output)	$P_1$	$P_d$	$h_0$ (m)	$h_1$ (m)	$B_1$ (m)	$v$ (m/s)	$Q_0$ (m <sup>3</sup> /s)
Value	26.54	26.81	1.55	3.40	5.47	5.50	52.08

As show in Fig. 14, the example bend is located in the middle reaches of the Fencha Gully, because of long-term erosion by debris flow, the bend characteristics are recognizable and the bend channel presents a relatively regular arc shape. A significant mountain landslide has appeared on the upper side of the concave bank. This phenomenon can be attributed to continuous erosion occurring on the concave bank, which induces a persistent collapse of the mountain slope above the concave bank. The channel width is 6 m, the curvature radius is 20 m, and the longitudinal slope of the channel is 297 %.

Based on the calculation method proposed in Chapter 3.2, the calculation parameters are shown in the Table 3. We calculated the discharge of debris flow in the Fencha Gully which is 54.44 m<sup>3</sup>/s under the condition of 50-year return period. The debris flow discharge calculated through the terrain parameters of the bend is 52.08 m<sup>3</sup>/s, which indicates this estimation method is reliable.

## 6 Conclusions

This is a complex motion process of debris flows within a bend channel, the speed and direction constantly changing, existing research methods struggle to accurately describe this process. Therefore, in this study, it is assumed that the flow velocity of debris flow remains constant and that linear motion has completely transformed into centrifugal motion. Consequently, the centrifugal force could be equated to the normal stress on the channel bank. Although this method has certain limitations, it still has practical significance for roughly estimating the shear force of debris flow and the resistance force of the bank soil. The powerful erosion effect of debris flow induces severe erosion on the concave bank, which would trigger a series of geological disasters. Based on field investigations and laboratory experiments, the main concluding remarks are:

(1) Through laboratory experiments, we have derived the calculation method for the centrifugal force

exerted on the concave bank by debris flow.

(2) The significant fluctuations in debris flow discharge would result in a broader impact range on channel’s landforms compared to streams. The intense erosion caused by debris flow on the concave bank leads to an increase in bend curvature radius, while the destruction of the slope foot would trigger landslide disasters.

(3) The terrain parameters of the bend channels at the downstream can reflect the discharge pattern of debris flow. When the increase in curvature of the bend makes it impossible for the debris flow to further erode and damage the concave bank, the relationship between debris flow discharge and terrain evolution would exhibit an equilibrium state. Then we can use the terrain parameters of the bend at the downstream to calculate the discharge of debris flow.

## Acknowledgments

This study was funded by the National Natural Science Foundation of China (Grant No.42201095), the Second Tibetan Plateau Scientific Expedition and Research (STEP) Program (Grant No. 2019QZKK0902), and the Postdoctoral Special Funding Project of Sichuan Province (Funding No. TB2023028). The authors are thankful to Mr. Chen Shunli for his contribution to the preparation and implementation of the laboratory experiments.

## Author Contribution

Lu Ming is responsible for conducting model experiments, data analysis, and manuscript writing. Liu Jinfeng is responsible for guiding, supervising, and providing financial support, while Sun Hao is responsible for guiding and proposing revision suggestions. Abrar Hussain is responsible for correcting grammar errors. Shang Yuqi and Fu Hang were responsible for assisting Lu Ming in conducting model experiments.



## Ethics Declaration

**Availability of Data/Materials:** Data supporting this Research article are available from the

corresponding author on request.

**Conflict of Interest:** The authors declared that they have no conflicts of interest to this work.

## References

- Armanini A, Capart H, Fraccarollo L, et al. (2005) Rheological stratification in experimental free-surface flows of granular-liquid mixtures. *J Fluid Mech* 532: 269-319.  
<https://doi.org/10.1017/S0022112005004283>
- Beltaos S, Rajaratnam N (1973) Plane turbulent impinging jets. *J Hydraul Res* 11(1): 29-59.
- Chen NS, Yue ZQ, Cui P, et al. (2007) A rational method for estimating maximum discharge of a landslide-induced debris flow: a case study from southwestern China. *Geomorphology* 84(1-2):44-58.  
<https://doi.org/10.1016/j.geomorph.2006.07.007>
- D'Ambrosio D, Iovine G, Spataro W, et al. (2007) A macroscopic collisional model for debris-flows simulation. *Environ Modell Softw* 22(10): 1417-1436.  
<https://doi.org/10.1016/j.envsoft.2006.09.009>
- Doi, I, Matsuura S, Osawa H, et al. (2020) Effects of coastal erosion on landslide activity revealed by multi-sensor observations. *Earth Surf Proc Land* 45(10): 291-299.  
<https://doi.org/10.1002/esp.4880>
- Dowling CA, Santi PM (2014) Debris flows and their toll on human life: a global analysis of debris-flow fatalities from 1950 to 2011. *Nat Hazards* 71: 203-227.  
<https://doi.org/10.1007/s11069-013-0907-4>
- Frank F, McArdell BW, Huggel C, et al. (2015) The importance of entrainment and bulking on debris flow runout modeling: examples from the Swiss Alps. *Nat Hazard Earth Sys* 15(11): 2569-2583.  
<https://doi.org/10.5194/nhess-15-2569-2015>
- Gonzalez-Diez A, Remondo J, Diaz de Teran, et al. (1999) A methodological approach for the analysis of the temporal occurrence and triggering factors of landslides. *Geomorphology* 30: 95-113.  
[https://doi.org/10.1016/S0169-555X\(99\)00047-1](https://doi.org/10.1016/S0169-555X(99)00047-1)
- Haas T, McArdell BW, Nijland W, et al. (2022) Flow and bed conditions jointly control debris - flow erosion and bulking. *Geophys Res Lett* (10):49.
- Han Z, Chen G, Li Y, et al. (2015) Assessing entrainment of bed material in a debris - flow event: a theoretical approach incorporating monte carlo method. *Earth Surf Proc Land* 40(14):1877-1890.  
<https://doi.org/10.1002/esp.3766>
- Hsu L, Dietrich WE, Sklar L S (2008) Experimental study of bedrock erosion by granular flows. *J Geophys Res.* 113.F2.  
<https://doi.org/10.1029/2008JF001048>
- Hu KH, Cui P, You Y, et al. (2010) Nonlinear modified flood method for calculating the debris-flow peak discharge in Wenchuan earthquake region. *Advanced Engineering Sciences* 42(5):52-57.  
[https://doi.org/10.1016/S1876-3804\(11\)60004-9](https://doi.org/10.1016/S1876-3804(11)60004-9)
- Iverson, Richard M (2012) Elementary theory of bed-sediment entrainment by debris flows and avalanches. *J Geophys Res* 117: F03006.  
<https://doi.org/10.1029/2011jfo02189>
- Kean JW, Coe JA, Coviello V, et al. (2015) Estimating velocities of debris flow entrainment from ground vibrations. *Geophys Res Lett* 42(15):6365-6372
- Kim N, Nakagawa H, Kawaike K, et al. (2019) Estimation of debris flow discharge coefficient considering sediment concentration. *J Sediment Res* 34(1):7.  
<https://doi.org/10.1016/j.ijsrc.2018.05.003>
- Kothyari UC (2001) Scour around spur dikes and bridge abutments. *J Hydraul Res* 39(4): 367-374.  
<https://doi.org/10.1080/00221680109499841>
- Lacoste A, Vendeville BC, Loncke L (2011). Influence of combined incision and fluid overpressure on slope stability: experimental modelling and natural applications. *J Struct Geol* 33 (4): 731-742.  
<https://doi.org/10.1016/j.jsg.2011.01.016>
- Larsen M (2012) Landslide erosion coupled to tectonics and river incision. *Nat Geosci* (7): 468-473.  
<https://doi.org/10.1038/ngeo1479>
- Pan HL, Huang JC, Ou GQ (2015) Mechanism of downcutting erosion of debris flow over a movable bed. *J Mt Sci* 12(1).  
<https://doi.org/10.1007/s1162-012-2523-2>
- Prochaska A (2005) Sensitivity and appropriateness of debris flow runup and superelevation equations. debris-flow processes, stratigraphy, geomorphology, and societal response.
- Rickenmann D, Weber D, Stepanov B (2003) Erosion by debris flows in field and laboratory experiments. *International Conference on Debris-Flow Hazards Mitigation: Mechanics, Prediction, and Assessment, Proceedings* (2003) 2 883-894
- Roelofs L, Colucci P (2022) How debris-flow composition affect bed erosion quantity and mechanisms: an experimental assessment. *Earth Surf Proc Land* 1-19.  
<https://doi.org/10.1002/esp.5369>
- Scheidl C, McArdell B, Rickenmann D (2015) Debris-flow velocities and superelevation in a curved laboratory channel. *Can Geotech J* 52(3):1-13.  
<https://doi.org/10.1139/cgj-2014-0081>
- Schürch P, Densmore A, Rosser N, et al. (2011) Dynamic controls on erosion and deposition on debris-flow fans. *Geology* 39(9): 827-830.  
<https://doi.org/10.1130/g32103.1>
- Stoffel M, Mendlik T, et al. (2014) Possible impacts of climate change on debris-flow activity in the Swiss Alps. *Climatic Change* 122(1-2): 141-155.  
<https://doi.org/10.1007/s10584-013-0993-z>
- Zheng H, Shi Z, De Haas T, et al. (2022) Characteristics of the impact pressure of debris flows. *J Geophys Res* 127.  
<https://doi.org/10.1029/2021JF006488>
- Zheng H, Shi Z, Peng M, et al. (2018) Coupled CFD-DEM model for the direct numerical simulation of sediment bed erosion by viscous shear flow. *Eng Geol* 245: 309-321.  
<https://doi.org/10.1016/j.enggeo.2018.09.003>
- Zheng H, Shi Z, Yu S, et al. (2021) Erosion mechanisms of debris flow on the sediment bed. *Water Resour Res* 57(12).  
<https://doi.org/10.1029/2021WR030707>